



Virus Capture Hot Paper

How to cite: *Angew. Chem. Int. Ed.* **2021**, *60*, 23756–23762

International Edition: doi.org/10.1002/anie.202108951

German Edition: doi.org/10.1002/ange.202108951

Polarity-Dominated Stable N97 Respirators for Airborne Virus Capture Based on Nanofibrous Membranes

Qifei Wang, Yingzhen Wei, Wenbo Li, Xizi Luo, Xinyue Zhang, Jiancheng Di, Guoqing Wang, and Jihong Yu*

Abstract: The longevity and reusability of N95-grade filtering facepiece respirators (N95 FFRs) are limited by consecutive donning and disinfection treatments. Herein, we developed stable N97 nanofibrous respirators based on chemically modified surface to enable remarkable filtration characteristics via polarity driven interaction. This was achieved by a thin-film coated polyacrylonitrile nanofibrous membrane (TFPNM), giving an overall long-lasting filtration performance with high quality factor at 0.42 Pa^{-1} (filtration efficiency: over 97%; pressure drop: around 10 Pa), which is higher than that of the commercial N95 FFRs ($0.10\text{--}0.41 \text{ Pa}^{-1}$) tested with a flow rate of 5 L min^{-1} and the $0.26 \mu\text{m}$ NaCl aerosol. A coxsackie B4 virus filtration test demonstrated that TFPNM also had strong virus capture capacity of 97.67%. As compared with N95 FFRs, the TFPNM was more resistant to a wider variety of disinfection protocols, and the overall filtration characteristics remained N97 standard.

Introduction

Filtering facepiece respirators (FFRs) have become a global protection pathway with the air pollution growing as a worldwide concern. Polluted air contained particular matter (PM) not only leads to health threat to people, but also influences climate and ecosystems.^[1] Aimed at $\text{PM}_{2.5}$ and PM_{10} (particle size below 2.5 and 10 μm , respectively), membrane-based air filters have been explored to capture the PM from polluted air.^[1a,2] However, for dangerous airborne particulates, including viral aerosols, the conventional air filters could not enable efficient filtration of these particulates.

In 2019, a respiratory disease broke out and developed into a rapid spread impact across the globe with more than 200 countries involved. This fatal disease is named as

Coronavirus disease 2019 (COVID-19), which is a universal pandemic caused by the novel severe acute respiratory syndrome coronavirus 2 (SARS-CoV-2). The size of COVID-19 virus is at 60–140 nm.^[3] It has been authoritatively demonstrated that the dominant transmittance route of COVID-19 is from infected individuals while coughing, sneezing and talking to uninfected people through the inbreathing of droplets or aerosols in the air.^[4] For these dangerous airborne particulates, the N95 FFR is recommended to be used as personal protective equipment for healthcare aim, which is typically constructed by multiple layers of charged polypropylene (PP) fibers with diameters between 1–10 μm .^[5] According to the announcement published by the United States Centers for Disease Control and Prevention's (CDC's) National Institute of Occupational Safety and Health (NIOSH) (document 42 CFR Part 84),^[6] N95 is assigned to a filtration efficiency reached to or over 95% on 0.3 μm sized sodium chloride (NaCl) aerosols. The N95 FFRs have been professionally confirmed that their filtration efficiency should be adequate for daily protection.^[5,7] Structurally, the micro-sized PP fibers are meltblown to build a lofty nonwoven with large void space and high layer thickness to provide sufficient physical barriers, but the high layer thickness would cause the increase of the corresponding pressure drop. To further improve the filtration efficiency and keep a relatively low resistance, the PP fibers are charged via corona discharge method to afford the N95 FFRs strong particulate adhesion via electrostatic charges (Figure 1a).^[8] However, the charges could degrade during respiration, leading to a concomitant drop in filtration efficiency during use.^[9] Furthermore, the N95 FFRs would be limited for reuse considering hygiene, damage, increased breathing resistance and the decreased filtration efficiencies.^[9,10] To develop the healthy and safe reuse of the membrane-based respirators, the CDC has recommended effective disinfection treatments and sterilization methods, including chemical, thermal and radiative strategies. The proper disinfection techniques, such as heat treatments, are promising and nondestructive strategies to keep the filtration characteristics of N95 FFRs. However, solution-based disinfection methods could significantly degrade the filtration efficiency of N95 FFRs to unacceptable grade,^[5] as these liquid-involved conditions would cause an inevitable corrosive effect to the surface electrostatic charges.^[11]

Considering the problems that the existing charged respirator membranes could not overcome the aforementioned disadvantages, it is important to develop a facile approach to realize high filtration efficiency and stability.

[*] Q. Wang, Y. Wei, W. Li, Dr. J. Di, Prof. J. Yu
State Key Laboratory of Inorganic Synthesis and Preparative
Chemistry, College of Chemistry, Jilin University
Changchun 130012 (P. R. China)
E-mail: jihong@jlu.edu.cn

Prof. J. Yu
International Center of Future Science, Jilin University
Changchun 130012 (P. R. China)

X. Luo, X. Zhang, Prof. G. Wang
Department of Pathogenbiology, Chinese Ministry of Education,
College of Basic Medicine, Jilin University
Changchun, 130021 (P. R. China)

Supporting information and the ORCID identification number(s) for the author(s) of this article can be found under:
<https://doi.org/10.1002/anie.202108951>.

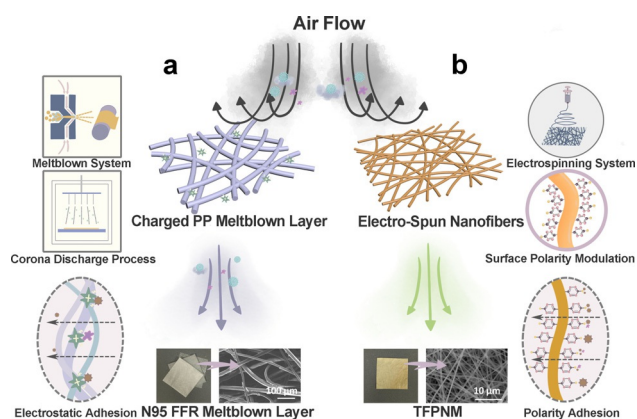


Figure 1. Illustration of overall characteristics and particulates capture mechanism of N95 FFR and TFPNM. a) Electrostatic charges-dominated N95 FFR. In commercial N95 FFRs, the fine particles are able to pass through the filter layers (charged meltblown PP fabrics), while most particles could be captured in the case of electret. b) Polarity-dominated TFPNM. The TFPNM can effectively capture most fine particles through polarity interaction.

Inspired by the particulate adhesion that could be manipulated by the surface chemistry of the membrane,^[1a,12] herein a polarity-dominated filtration approach based on nanofibrous membranes has been enlightened to enable remarkable filtration characteristics reaching to N97 grade with outstanding longevity and reusability (Figure 1 b). Compared with electrostatic governed membranes, the chemically optimized membranes can not only afford strong surface adhesion, but also keep a long-lasting filtration efficiency in terms of stable surface chemistry by meanwhile decreasing the fiber diameter to nano size.^[13] Followed by this design protocol, in this work, a thin-film (TF) coated electrospun polyacrylonitrile (PAN) nanofibrous membrane (TFPNM) has been introduced. The highly polar TF layer was uniformly post-modified on every single nanofiber, leading to remarkable anti-corrosion performance in various harsh conditions and strong particulate adhesion. Significantly, the TFPNM exhibited much stronger affinity to airborne particulates via polar–polar interaction between the membrane and PMS/aerosol. The TFPNM was also successfully applied in airborne virus capture, exhibiting striking capture capability. Moreover, the stable and strong surface polarity of TFPNM enabled their safety reuse upon diverse disinfection treatments, even solution-based disinfection conditions. The PAN is available in large quantity and at low cost, making TFPNM great commercial potential as respirator membranes. Such a facile polar membrane-based respirator would realize a highly efficient and stable air filtration and develop opportunities to achieve much more effective personal healthcare.

Results and Discussion

The TF coated PAN nanofibrous membranes (TFPNMs) were fabricated via electrospinning technique, and functionalized through an interfacial polymerization process, resulting

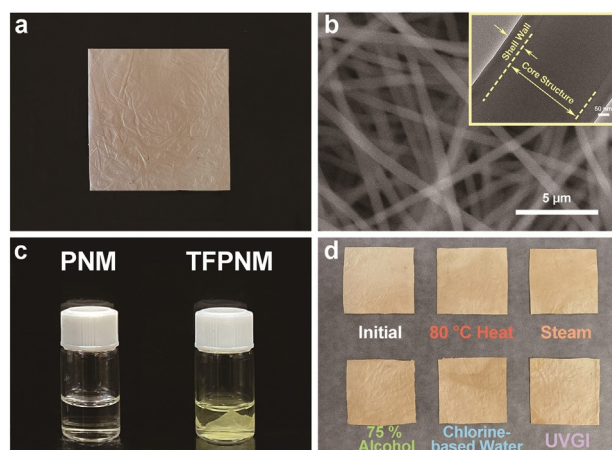


Figure 2. The morphology and stability of TFPNMs. a) Digital Image of cTFPNM (3.5 cm × 3.5 cm). b) SEM image and inserted TEM image of cTFPNM, displaying a nano-sized core–shell structure. c) Stability of PNM and cTFPNM in dimethylformamide (DMF). The PNM was completely dissolved in DMF solution (left bottle) within 5 min, while the cTFPNM remained stable in DMF solution after soaking for 90 days. d) The cTFPNMs treated in various harsh conditions. The initial morphology was well maintained, indicating that the TF layer enabled high stability of TFPNMs. cTFPNM: 4-carboxyl-ph-terminated TFPNM.

in light-yellow fabrics with alterable terminal groups (Figure 2 a). The details of the polymerization process have been reported earlier.^[13c] As shown in Figure 2 b, the scanning electron microscopy (SEM) image displays an intertwined fibrous morphology, and the thin-film layer forms a uniform shell over the PAN nanofibers as revealed in the transmission electron microscopy (TEM) image. After the coating process, the TFPNM remains an intertwined fibrous structure with the mean fiber diameter increasing from 400–500 nm to 500–600 nm (Supporting Information, Figure S1). Figure S2 shows the geometries of the TFPNMs with different terminal groups, indicating no morphological changes on the fibers after modification. The alteration of the terminal groups results in a great difference in the surface tension of TFPNMs, as well as the surface polarity. As previously reported by Fowkes,^[14] the surface tension is composed of two independent parts: 1) a dispersive part (γ_s^d) and 2) a polar part (γ_s^p). The γ_s^p values were precisely calculated via Owens-Wendt-Rabel-Kaelble (OWRK) method for each TFPNM as compared with meltblown PP fabrics.^[15] The γ_s^p value of PP was calculated as $0.18 \pm 0.18 \text{ mJ m}^{-2}$, indicating that PP meltblown fabrics is a nonpolar material. Compared with PP, the TFPNMs possessed much stronger surface polarity, which could be altered through different coatings from 2.99 mJ m^{-2} (4-trifluoromethoxy-Ph-TF) to 66.09 mJ m^{-2} (4-carboxyl-Ph-TF) as shown in Supporting Information, Table S1. The TF layer also showed a strong resistance in the organic solvents (Figure 2 c and Supporting Information, Figure S3), which allowed the exposure of TFPNM in harsh solvent environments. To further estimate the stability of the TFPNMs, the membranes were exposed in various conditions, including high temperature (over 80 °C), steam atmosphere (over 100 °C with high humidity), 75% alcohol, chloride-based disinfecting water and Ultraviolet (UV) light. There was no

apparent damage and weight loss on the TFPNMs (Figure 2d), indicating no changes occurred on the fibrous geometry. The surface polarity of the TFPNMs upon these harsh treatments was evaluated. Compared with the initial TFPNM, the surface polarity of post-treated TFPNMs remained unchanged as shown in Supporting Information, Table S2. The stable surface polarity can enable stable polar-polar interaction between the membrane and PMs/aerosol, promising the TFPNMs great potential of reusability in various harsh conditions.

We firstly examined the capture capability of TFPNMs for various sizes of particulate matters (PMs) in order to simulate the air filtration in hazardous air-quality conditions. The burning incense was used in the laboratory to present hazardous PM level, which contains varieties of contaminants (PM, CO, CO₂, NO₂ and etc.).^[1a,2a,16] Figure 3a reveals the relationship between the pressure drop of TFPNMs and their basis weight and air flow. As can be seen, the increasing of the membrane thickness and the wind resistance could result in an apparent growth of pressure drop over the membranes. To keep a low resistance under high air flow (> 5 L min⁻¹), the optimal basis weight of all the TFPNMs was controlled at 10 g m⁻². Notice that, in Figure 3b, five TFPNMs with different surface polarity exhibit a large difference in the filtration efficiency. The relative results vary from 50.00 % to 97.45 % at PM_{0.3}, according to the surface polarity from the lowest to the highest. It further confirms that the polar-polar interaction plays a dominant role in the PMs capture capability. Notably, the TFPNMs with cyano group and carboxyl group exhibit

remarkably high filtration efficiency even over 97 % (Figure 3b). To study the long effectiveness of the TFPNMs, the 4-cyan-ph-terminated TFPNM (CTFPNM), which possesses the same terminal group (-CN) as PAN molecule does, was tested in a continuous 10 h filtration process under a hazardous air-quality condition (with PM_{2.5} concentration > 1000 μg m⁻³, PM_{2.5} number density > 17650 per m³). The results show great distinction between PAN nanofibrous membrane (PNM) and CTFPNM in the corresponding filtration efficiencies (Figure 3c). As for PNM, the filtration efficiency for PM_{0.3} degraded from 97.10 % to 94.57 % and the filtration efficiency degraded from 99.67 % to 99.42 % for PM_{2.5} after 10 h. However, the filtration characteristic of CTFPNM remained stable, with filtration efficiencies over 97.00 % and 99.90 % for PM_{0.3} and PM_{2.5}, respectively, in 10 h.

Furthermore, CTFPNM and 4-carboxyl-ph-terminated TFPNM (cTFPNM) show outstanding filtration characteristics, especially the longevity, in a 24 h continuous blocking test with PM_{10-2.5} filtration efficiencies reaching to 99.90 % (Supporting Information, Figure S4). A direct demonstration of the blocking of PMs over a TFPNM is shown in Figure 3d. The TFPNM (3.5 cm × 3.5 cm) was tightly fixed in the middle of two flanges, with the PM_{2.5} concentration over 1000 μg m⁻³ in the left bottle. As shown in Figure 3d, the right bottle could remain clear with the PM_{2.5} concentration in a superior level (< 1 μg m⁻³) after 1 h.

To study the filtration characteristics of TFPNMs compared with N95 FFRs, two TFPNMs with high surface polarity, CTFPNM and cTFPNM, were introduced for cubic NaCl aerosols filtration. All the TFPNM samples with the same basis weight at 10 g m⁻² were characterized with a flow rate of 5 L min⁻¹ and the NaCl (0.26 μm medium diameter) aerosol. As shown in Figure 4a and Supporting Information, Figure S5a, the filtration efficiencies of both CTFPNM and cTFPNM achieve at N97 grade and remain steady within a continuous 24 h filtration process. The basis weights of both TFPNMs increase to 13 g m⁻² due to the loading of NaCl aerosols within 24 h, which results in a slight increase of the corresponding pressure drops from 9–10 Pa to around 13 Pa (Figure 4b and Supporting Information, Figure S5b). The relatively low pressure drop demonstrates an appropriate respiratory resistance, giving the practicability of TFPNM applied as a filtering facepiece respirator. By contrast, N95 FFRs dominated by charged PP meltblown fabrics show obvious instability during filtering. As shown in Figure 4c, d, for the filtering layers of MEO-brand and 3Q-brand N95 FFRs, around 80 % electrostatic charges broke away within 10 h. The remaining charges at 10–15 % (0.20–0.30 kV) can still capture aerosols in the following 14 h, but the filtration efficiencies for N95 FFRs dropped below 95 %. Meanwhile, when loading with more NaCl aerosols for 24 h, the N95 FFRs have an obvious increase of the pressure drops from 8 Pa to 15 Pa for MEO-brand and from 15 Pa to 25 Pa for 3Q-brand. The electrostatic effect was further studied on the filtration efficiencies of the TFPNMs. Their filtration efficiencies exhibit a slight increase to N98 grade for both charged cTFPNM and CTFPNM (Supporting Information, Figure S5c, d). However, the filtration efficiencies of these charged respirator membranes finally drop to N97 grade after

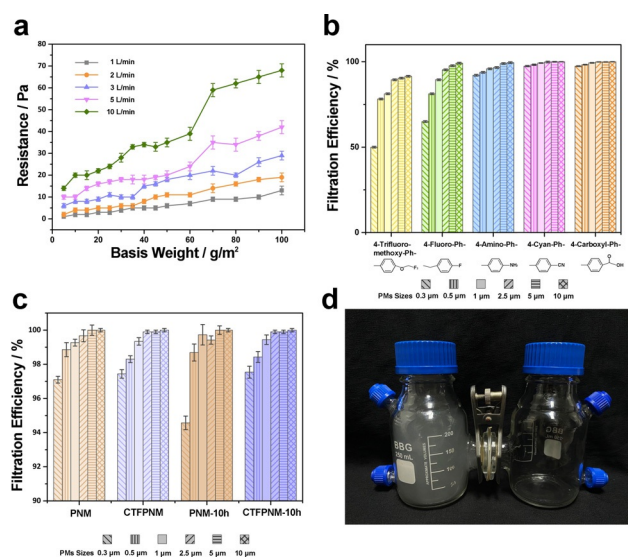


Figure 3. Performance of PMs capture over TFPNMs with different surface polarity. a) Impact on the pressure drop of cTFPNM. The basis weight of cTFPNM and flow rate both exhibit notable impact on the value of pressure drop. The TFPNM with basis weight at 10 g m⁻² was applied in all filtration experiments. b) Filtration efficiency comparison between TFPNMs with different terminal groups: 4-trifluoro-methoxy-Ph, 4-fluoro-Ph, 4-amino-Ph, 4-cyan-Ph, and 4-carboxyl-Ph. c) Durability test between PNM and CTFPNM within 10 h filtration cycles. d) Demonstration of TFPNM blocking PM from the outdoor (left bottle, PM_{2.5} concentration > 1000 μg m⁻³) to the indoor (right bottle, PM_{2.5} concentration < 1 μg m⁻³) environment.

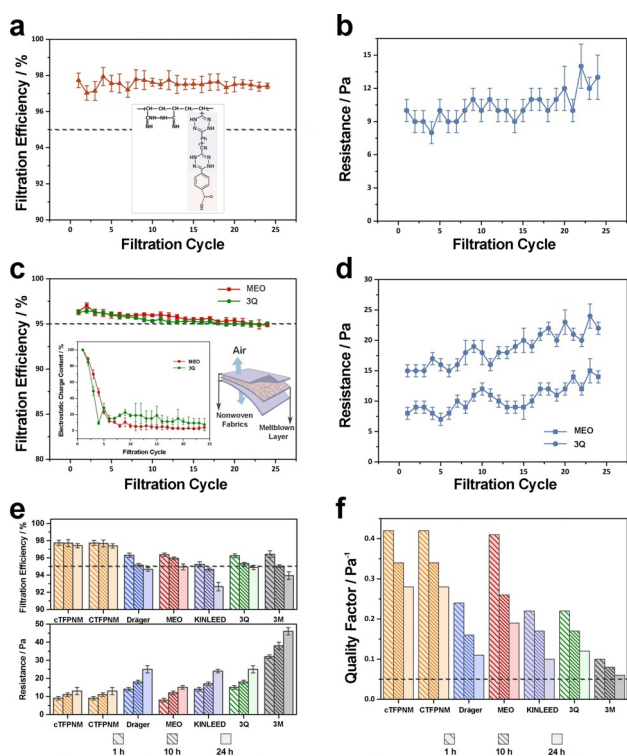


Figure 4. Filtration characteristics of TFPNMs and the filtering layers of multiple brands N95 FFRs. A 24 h evolution of respirator's filtration characteristics, filtration efficiencies and the corresponding pressure drops of uncharged cTFPNM (a) and (b) and commercial N95 FFRs (MEO and 3Q) (c) and (d). For the inserted Figure in c, there is a loss on the electrostatic charges during the filtration process. The content of the electrostatic charges remained 10–20% after 10 h, and 10–15% after 24 h, which still allowed the N95 FFRs to capture aerosols. e) A 24 h evolution of multiple FFRs' filtration characteristics at room temperature, filtration efficiencies and pressure drops. f) The quality factor (QF) represents the overall filtration performance of various respirator membranes.

24 h due to the decay of the surface electrostatic charges (from 0.15 kV to 0.02 ± 0.03 kV). Because of the sustained surface polarity, the filtration efficiencies can be maintained at 97% after 24 h. We further investigated the superiority of TFPNMs on air filtration characteristics as compared with various N95 FFRs from different countries, which all show a degradation on filtration efficiencies below 95% after 24 h continuous filtration (Figure 4e): (1) Dräger X-plore 1095 (France, GB2626 KN95, from 96.31% to 94.67%), (2) MEO (New Zealand, AS/NZS KN95, from 96.37% to 94.84%), (3) KINLEED (China, GB2626 KN95, from 95.25% to 92.66%), (4) 3Q (China, GB19083 N95, from 96.25% to 94.89%) and (5) 3M 8210 (The United States, NIOSH N95, from 96.42% to 93.94%). It can be seen in Figure 4e, the filtration efficiencies of N95 FFRs are all below the filtration efficiency of cTFPNM at 97.42% under the same experimental conditions after 24 h. The basis weights of the filtering layer of N95 FFRs were also measured: (1) Dräger X-plore 1095 (60.60 gm^{-2}), (2) MEO (28.67 gm^{-2}), (3) KINLEED (60 gm^{-2}), (4) 3Q (65.85 gm^{-2}) and (5) 3M 8210 (341.20 gm^{-2}). Their high packing density results in a high respiratory resistance even reaching to 32 Pa (3M-brand)

(Figure 4e). By contrast, the TFPNM possesses stable filtration efficiency at N97 level via strong surface polar interaction even without external charges, and the pressure drop remains comparable (below 13 Pa) for long periods, indicating its commercial potential for practicability.

The quality factor (QF) was introduced to estimate the overall performance of membrane-based respirators, considering both the filtration efficiency and the pressure drop.^[17] It is expressed as:

$$QF = -\frac{\ln(1-\eta)}{\Delta p} \quad (1)$$

Where η represents the filtration efficiency, Δp is the pressure drop value under certain flow rate. The QF is universally used according to the WHO and recommended to be ranged over 0.05 Pa^{-1} .^[18] The overall filtration characteristics of the aforementioned respirators were investigated as shown in Figure 4f, and the corresponding QFs were calculated and summarized in Supporting Information, Table S3. For the N95 FFRs, the filtration efficiencies drop below 95% due to the decay of the electrostatic charges and the pressure drops meanwhile keep increasing in 24 h, leading to the poor filtration performances. Taking MEO-brand N95 FFR as an example, which shows a much higher QF than the other N95 FFRs, it has a great change in the QF in 24 h. When a large quantity of electrostatic charges apparently decays after 10 h, the QF degrades from 0.41 Pa^{-1} to 0.26 Pa^{-1} , and then drastically degrades to 0.19 Pa^{-1} in 24 h due to the insufficient physical barriers provided by PP meltblown fabrics. Other N95 FFRs show a similar change in the QFs. By contrast, the TFPNMs possess superior and more stable filtration characteristics. The initial QFs for both cTFPNM and CTFPNM are 0.42 Pa^{-1} , owing to the N97 grade filtration efficiency and relatively low pressure drop. After 10 h, the advantage of polarity-dominated TFPNMs on overall filtration performances becomes much more obvious with QFs at 0.34 Pa^{-1} compared to the N95 FFRs with a lack of electrostatic charges (possessing poor QFs at 0.08 Pa^{-1} to 0.26 Pa^{-1}). After 24 h, the pressure drops of TFPNMs can be maintained at around 13 Pa, and the filtration efficiencies keep comparable at N97 grade, therefore, the QFs of TFPNMs can reach to 0.28 Pa^{-1} . While the QFs for N95 FFRs appreciably drop to 0.06 Pa^{-1} to 0.19 Pa^{-1} , owing to the unstable filtration efficiencies and relatively high pressure drops.

The cTFPNM (basis weight of 10 gm^{-2}) was deployed in viral aerosols to evaluate its filtration efficiency. The isolated small viruses could be more difficult to capture due to their teeny sizes. For example, the sizes of the picornaviruses are around 30 nm ^[19] and the mean diameter of influenza viruses is around 120 nm .^[20] All these particulates with diameter under $0.3 \mu\text{m}$ are neglected in conventional filtration efficiency tests. In this work, we employed an infectious virus, Coxsackie B4 virus (CV-B4), a tiny RNA virus ($27\text{--}30 \text{ nm}$), into the filtration system.^[21] The viral solution was aerosolized at $0.26 \mu\text{m}$ medium diameter with a flow rate of 5 Lmin^{-1} throughout the filtration test. We also performed viral filtration test over MEO-brand N95 FFR, to investigate its virus capture capability. As shown in Figure 5a, the cTFPNM

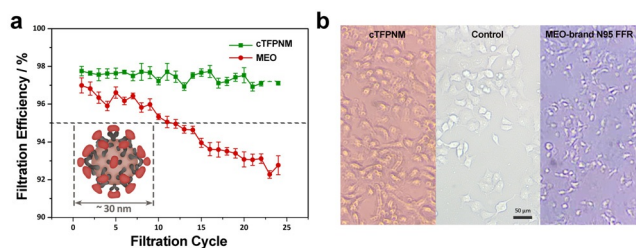


Figure 5. Filtration performance for virus over cTFPNM. a) A 24 h evolution of cTFPNM's and MEO N95 FFR's filtration efficiencies for CV-B4 virus at room temperature. b) Cytopathic effects mediated by the CV-B4 virus extracted from the filtered CV-B4 viral aerosols over cTFPNM (left) and MEO-brand N95 FFR (right) after a continuous 24 h filtration process, both compared with the healthy HeLa cells (middle). The HeLa cells propagated with CV-B4 virus were cultured for 5 days and observed with light microscope.

remains N97-grade filtration efficiency up to 24 filtration cycles while the filtration efficiency of MEO-brand N95 FFR degrades below 95% after 24 h.

To estimate the virus penetrability across the respirator membranes, we studied the cytopathic effect (CPE) of CV-B4 in the HeLa cells.^[22] As shown in Figure 5b, most HeLa cells propagated in the filtered CV-B4 viral aerosols over cTFPNM remain a relatively polyhedral cell shape (left image), as compared with the healthy HeLa cells (middle image). However, the CV-B4 virus in the compressed filtered aerosols over MEO-brand N95 FFR can apparently cause the CPE of most HeLa cells (right image), leading to cell shrinkage, rounding and a cell release from the monolayer.^[23] This is because that most viruses could be successfully captured over TFPNM, yet the N95 FFR has insufficient capture capability of tiny viral aerosols (Supporting Information, Figure S6). Further virus titration test gave a degradation on the virus concentration from 10^3 to 10^1 TCID₅₀/0.1 mL over cTFPNM, also demonstrating its remarkable virus capture capability.

To investigate the reusability of TFPNMs, five commonly home-exercisable methods were operated on cTFPNMs:^[24] (1) heat treatment with temperature at 80 °C (High temperature above 70 °C could lead to protein denaturation of SARS-CoV-2 over 5 min);^[25] (2) steam (100 °C heat-based protein denaturation); (3) 75% alcohol (protein denaturation);^[26] (4) domestic chlorine-based solution (cellular denaturation, with chemical damage);^[27] (5) ultraviolet germicidal irradiation (DNA/RNA disruption, UVC 254 nm).^[28] As seen in Supporting Information, Table S4, all the filtration efficiencies remain unchanged at N97 level after the first treatment cycle with pressure drops maintained at 9–10 Pa. The geometry and loftiness of the cTFPNMs are unchanged (Supporting Information, Figure S7) and the surface polarities keep comparable (Supporting Information, Table S1), which further demonstrates that the TFPNMs are stable for reuse. In contrast, the N95 FFRs show different filtration performances upon various treatments after the first cycle. As seen in Supporting Information, Table S5, heating and ultraviolet germicidal irradiation (UVGI) can preserve the filtration characteristics for most N95 FFRs. However, the filtration efficiencies drastically decrease to 50–80% upon solu-

tion-based treatments with a complete degradation on electrostatic charge quantity to 0 kV, which is far beyond N95 grade. Taking the MEO-brand N95 FFR as an example, large pores randomly exist in the meltblown samples (Supporting Information, Figure S8), leading to an unacceptable filtration efficiency at 68.58% and 57.33% in 75% alcohol and chlorine-based solution, respectively. The corresponding pressure drops change from 8 Pa to 10 Pa (in 75% alcohol) and 5 Pa (in chlorine-based solution), respectively (Supporting Information, Table S6). As for Dräger-brand N95 FFR, the apparent degradation can be observed upon UVGI treatment, with the filtration efficiency decay to 93.82%.

We further investigated the stability of different respirators upon various disinfections in multiple treatment cycles, and the corresponding results after 10 cycles are illustrated in Figure 6. Significantly, the cTFPNM deposited upon various

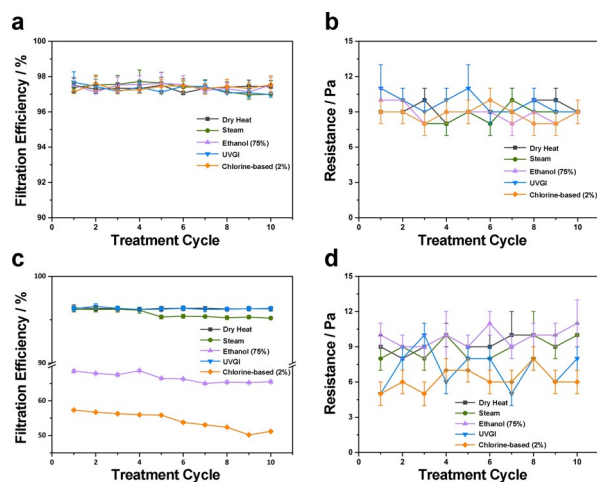


Figure 6. Evolution of FFRs upon five different disinfection treatments and corresponding overall filtration performance. The corresponding filtration efficiencies and pressure drops of cTFPNM (a and b) and MEO-brand N95 FFR (c and d). The cTFPNM remained N97 level after 10 treatment cycles, while the MEO-brand N95 FFR exhibited poor filtration characteristics especially in solution-based treatments.

disinfection treatments can maintain the corresponding filtration efficiencies at N97 level with pressure drops at 9–10 Pa after 10 cycles (Figure 6a, b). However, the MEO-brand N95 FFR exhibited poor recyclability in 10 cycles upon some disinfection treatments (Figure 6c, d). The filtration efficiencies were able to be retained over 95% after 10 cycles of heat and UVGI treatments. Treatments involving liquids and vapors, such as steam, alcohol, and household bleach, all led to degradation of the filtration efficiency, very likely due to the decay of the electrostatic charges, in addition to possible mechanical damage of the respirator membranes. Even worse, after 10 cycles, the MEO-brand N95 FFRs treated in both solution-based disinfection methods showed substantial degradation on filtration efficiencies to 65.52% (in 75% alcohol) and 51.18% (in chlorine-based solution).

Conclusion

We have developed a facile air filtration approach dominated by polarity interaction between the respirator membranes and the airborne PMs and aerosols. The electrospun PAN nanofibrous membranes with modified surface polarities (TFPNMs) give the air filtration N97 grade efficiency and show long effectiveness, excellent reusability and practicability as respirator membranes, which significantly overcome the disadvantages of the N95 FFRs caused by the unstable electrostatic charges. Compared with the charged nonpolar polypropylene (PP) microfibers, which capture the fine particulates mainly through electrostatic adhesion, the highly polar nanofibers in TFPNM have great capture capability of PMs and aerosols owing to the strong surface polarity. And the thin nanofibrous construction can provide strong physical barrier under low pressure drop, leading to remarkable practicability as FFRs. Furthermore, for PMs and aerosols under 0.3 μm , especially the dangerous viruses, the TFPNM enables more stable and highly efficient viral filtration compared with the N95 FFRs. Owing to the stably maintained surface polarity of TFPNMs, the filtration efficiency can keep at N97 grade upon multiple disinfection treatment cycles, including both physical and chemical methods. Therefore, the TFPNMs show great potential in achieving a healthy and safe reuse of the respirators for the public, having N97 grade filtration efficiency with prominent longevity, reuse potential and practicability. These advantages promise the polarity-dominated air filtration approach as a guidance in helping the public to raise the safety standard of using mask protection.

Acknowledgements

This work was supported by the National Natural Science Foundation of China (Grant Nos. 21920102005, 21835002 and 21621001), and the 111 Project of China (B17020).

Conflict of Interest

The authors declare no conflict of interest.

Keywords: materials science · N97 grade · reusability · thin films · virus capture

- [1] a) C. Liu, P. C. Hsu, H. W. Lee, M. Ye, G. Zheng, N. Liu, W. Li, Y. Cui, *Nat. Commun.* **2015**, *6*, 6205; b) W. Cai, G. Wang, A. Santoso, M. J. McPhaden, L. Wu, F.-F. Jin, A. Timmermann, M. Collins, G. Vecchi, M. Lengaigne, M. H. England, D. Dommenget, K. Takahashi, E. Guilyardi, *Nat. Clim. Change* **2015**, *5*, 132–137; c) J. Lelieveld, J. S. Evans, M. Fnais, D. Giannadaki, A. Pozzer, *Nature* **2015**, *525*, 367–371; d) D. Fang, B. Chen, K. Hubacek, R. Ni, L. Chen, K. Feng, J. Lin, *Sci. Adv.* **2019**, *5*, eaav4707.
- [2] a) B. Wang, Q. Wang, Y. Wang, J. Di, S. Miao, J. Yu, *ACS Appl. Mater. Interfaces* **2019**, *11*, 43409–43415; b) K. Liu, C. Liu, P. C. Hsu, J. Xu, B. Kong, T. Wu, R. Zhang, G. Zhou, W. Huang, J. Sun, Y. Cui, *ACS Cent. Sci.* **2018**, *4*, 894–898.
- [3] a) N. Zhu, D. Zhang, W. Wang, X. Li, B. Yang, J. Song, X. Zhao, B. Huang, W. Shi, R. Lu, P. Niu, F. Zhan, X. Ma, D. Wang, W. Xu, G. Wu, G. F. Gao, W. Tan, *N. Engl. J. Med.* **2020**, *382*, 727–733; b) Y. Zhu, D. Yu, Y. Han, H. Yan, H. Chong, L. Ren, J. Wang, T. Li, Y. He, *Sci. Adv.* **2020**, *6*, eabc9999; c) K. K. Chan, T. J. C. Tan, K. K. Narayanan, E. Procko, *Sci. Adv.* **2021**, *7*, eabf1738.
- [4] J. Leap, V. Villgran, T. Cheema, *Crit. Care Nurs. Q.* **2020**, *43*, 338–342.
- [5] L. Liao, W. Xiao, M. Zhao, X. Yu, H. Wang, Q. Wang, S. Chu, Y. Cui, *ACS Nano* **2020**, *14*, 6348–6356.
- [6] L. Rosenstock, *Infect. Control Hosp. Epidemiol.* **1995**, *16*, 529–531.
- [7] W. C. Hill, M. S. Hull, R. I. MacCuspie, *Nano Lett.* **2020**, *20*, 7642–7647.
- [8] a) R. Dennis, B. C. Pourdeyhimi, A. S. Emanuel, D. Hubbard, *J. Sci. Med. Sport* **2020**, *2*, 1; b) S.-H. Huang, C.-W. Chen, Y.-M. Kuo, C.-Y. Lai, R. McKay, C.-C. Chen, *Aerosol Air Qual. Res.* **2013**, *13*, 162–171.
- [9] E. Hossain, S. Bhadra, H. Jain, S. Das, A. Bhattacharya, S. Ghosh, D. Levine, *Phys. Fluids* **2020**, *32*, 093304.
- [10] a) CDC, “Coronavirus Disease 2019 (COVID-19). In: Centers for Disease Control and Prevention”, can be found under <https://www.cdc.gov/coronavirus/2019-ncov/hcp/respirator-use-faq.html>; b) C. D. Vuma, J. Manganyi, K. Wilson, D. Rees, *Ann. Work Expo. Health* **2019**, *63*, 930–936.
- [11] B. Cantaloube, G. Dreyfus, J. Lewiner, *J. Polym. Sci. Polym. Phys. Ed.* **1979**, *17*, 95–101.
- [12] J. Xu, C. Liu, P. C. Hsu, K. Liu, R. Zhang, Y. Liu, Y. Cui, *Nano Lett.* **2016**, *16*, 1270–1275.
- [13] a) S. Kuwabara, *J. Phys. Soc. Jpn.* **1959**, *14*, 527–532; b) S. A. Hosseini, H. V. Tafreshi, *Powder Technol.* **2010**, *201*, 153–160; c) K. W. Lee, B. Y. H. Liu, *Aerosol Sci. Technol.* **1981**, *1*, 35–46; d) J. Xue, T. Wu, Y. Dai, Y. Xia, *Chem. Rev.* **2019**, *119*, 5298–5415; e) Q. Wang, Y. Wang, B. Wang, Z. Liang, J. Di, J. Yu, *Chem. Sci.* **2019**, *10*, 6382–6389; f) J. Di, L. Li, Q. Wang, J. Yu, *CCS Chem.* **2020**, *2*, 2280–2297; g) L. Pérez-Manríquez, J. Aburabi'e, P. Neelakanda, K.-V. Peinemann, *React. Funct. Polym.* **2015**, *86*, 243–247.
- [14] a) F. M. Fowkes, *J. Phys. Chem.* **1962**, *66*, 382–382; b) F. M. Fowkes, *Ind. Eng. Chem.* **1964**, *56*, 40–52.
- [15] a) D. K. Owens, R. C. Wendt, *J. Appl. Polym. Sci.* **1969**, *13*, 1741–1747; b) D. H. Kaelble, *J. Adhes.* **1970**, *2*, 66–81.
- [16] a) B. Khalid, X. Bai, H. Wei, Y. Huang, H. Wu, Y. Cui, *Nano Lett.* **2017**, *17*, 1140–1148; b) T. C. Lin, G. Krishnaswamy, D. S. Chi, *Clin. Mol. Allergy* **2008**, *6*, 3.
- [17] C. D. Zangmeister, J. G. Radney, E. P. Vicenzi, J. L. Weaver, *ACS Nano* **2020**, *14*, 9188–9200.
- [18] Health Emergencies Preparedness and Response Team, *WHO*, **2020**.
- [19] M. G. Rossmann, E. Arnold, J. W. Erickson, E. A. Frankenbergger, J. P. Griffith, H. J. Hecht, J. E. Johnson, G. Kamer, M. Luo, A. G. Mosser, R. R. Rueckert, B. Sherry, G. Vriend, *Nature* **1985**, *317*, 145–153.
- [20] A. Harris, G. Cardone, D. C. Winkler, J. B. Heymann, M. Brecher, J. M. White, A. C. Steven, *Proc. Natl. Acad. Sci. USA* **2006**, *103*, 19123–19127.
- [21] a) L. Aguech-Oueslati, H. Jaidane, F. Sane, N. Jrad-Battikh, S. B. Hamed, D. Hober, J. Gharbi, *Curr. Microbiol.* **2018**, *75*, 32–39; b) H. Jmii, A. Halouani, M. Maatouk, L. Chekir-Ghedira, M. Aouni, S. Fisson, H. Jaïdane, *Microb. Pathog.* **2020**, *145*, 104235.
- [22] a) E. A. Govorkova, G. Murti, B. Meignier, C. de Taisne, R. G. Webster, *J. Virol.* **1996**, *70*, 5519–5524; b) M. A. Salako, M. J. Carter, G. E. Kass, *J. Biol. Chem.* **2006**, *281*, 16296–16304.
- [23] C. M. Carthy, D. J. Granville, K. A. Watson, D. R. Anderson, J. E. Wilson, D. Yang, D. W. C. Hunt, B. M. McManus, *J. Virol.* **1998**, *72*, 7669–7675.

- [24] a) A. W. H. Chin, J. T. S. Chu, M. R. A. Perera, K. P. Y. Hui, H.-L. Yen, M. C. W. Chan, M. Peiris, L. L. M. Poon, *Lancet Microbe* **2020**, *1*, e10; b) M. E. Darnell, K. Subbarao, S. M. Feinstone, D. R. Taylor, *J. Virol. Methods* **2004**, *121*, 85–91; c) H. F. Rabenau, J. Cinatl, B. Morgenstern, G. Bauer, W. Preiser, H. W. Doerr, *Med. Microbiol. Immunol.* **2005**, *194*, 1–6; d) D. J. Viscusi, M. S. Bergman, B. C. Eimer, R. E. Shaffer, *Ann. Occup. Hyg.* **2009**, *53*, 815–827.
- [25] P. N. Lelie, H. W. Reesink, C. J. Lucas, *J. Med. Virol.* **1987**, *23*, 297–301.
- [26] a) G. Kampf, D. Todt, S. Pfaender, E. Steinmann, *J. Hosp. Infect.* **2020**, *104*, 246–251; b) R. Thaper, B. Fagen, J. Oh, *Photochem. Photobiol. Sci.* **2021**, *20*, 955–965.
- [27] a) W. B. Salter, K. Kinney, W. H. Wallace, A. E. Lumley, B. K. Heimbuch, J. D. Wander, *J. Occup. Environ. Hyg.* **2010**, *7*, 437–445; b) C. Dellanno, Q. Vega, D. Boesenberg, *Am. J. Infect. Control* **2009**, *37*, 649–652.
- [28] D. Perdiz, P. Gróf, M. Mezzina, O. Nikaido, E. Moustacchi, E. Sage, *J. Biol. Chem.* **2000**, *275*, 26732–26742.

Manuscript received: July 6, 2021

Accepted manuscript online: August 26, 2021

Version of record online: September 22, 2021